Title here

Authors[a]

[a] *address*

Abstract

Keywords:

1. Introduction

Around the world traffic congestion causes a drain on the economy due to time and fuel wasted and collisions associated with traffic congestion. In 2011 congestion in America alone caused a loss of $121 billion due to 5.5 billion hours of extra travel time and 2.9 billion gallons of wasted fuel. Although congestion levels in America are much higher now than several decades ago, they have dropped below the peak in 2005, but will increase when the economy improves [1]. As personal vehicle ownership increases globally, traffic congestion continues to be a persistent problem. It is no surprise then that research in the physics of traffic developed with the ultimate goal of mitigating road traffic.

Traffic control strategies such as ramp metering and variable speed limits are in place today, but a good model of traffic dynamics is needed for proper coordination of control strategies. The 1950s saw the development of the Lighthill-Whitham-Richards (LWR) model [2] [3], which became the seminal model for traffic flow, still studied today. This model is a conservation law for vehicles, based on fluid dynamics. Yet as a first-order model it has inherent shortcomings, such as non-physical predictions of vehicle speed as a vehicle passes through a shock and the inability to describe jamitons, phantom traffic jams which seem to appear for no reason. This prompted the development of second-order models, the prototype of which is the Payne-Whitham (PW) model [4] [5]. This and later second-order models consist of two equations, the first being the LWR equation and the second a momentum equation analogous to that describing fluid flow. Daganzo later published a study of the serious flaws of second-order traffic models, namely the emergence of gas-like behavior. While the second-order models up to that point were able to capture physics that the LWR model could not, these improved models also lost the anisotropy of the LWR model, incorrectly predicting that vehicles are affected by vehicles from behind [6]. Soon after, Aw and Rascle, and independently Zhang, developed the ARZ model which avoided the inconsistencies of earlier higher-order models [7] [8].

2. The ARZ model

Aw and Rascle [7] and Zhang [8] independently developed a macroscopic second-order model of traffic flow to address the shortcomings of previously existing higher-order models. The (AR) model proposed by Aw and Rascle consists of the usual vehicle conservation and momentum equations:

$$\rho_t + (\rho v)_x = 0, \tag{1}$$

$$(v + p(\rho))_t + v(v + p(\rho))_x = 0, \tag{2}$$

where $v(x,t)$ and $\rho(x,t)$ are the density and velocity, respectively, and $p(\rho)$ is a smooth, increasing function analogous to the pressure term in fluid flow. Aw and Rascle demonstrate in [7] that "with a suitable choice of function p," the above class of models avoids inconsistencies of earlier second-order models. Zhang proposed in [8] the same model with $p(\rho) = -V(\rho)$, where $V(\rho) = Q(\rho)/\rho$ is the equilibrium velocity profile, and $Q(\rho)$ is the density-flow relation given by the fundamental diagram. In this paper we consider the Aw-Rascle-Zhang

(ARZ) model with a relaxation term:

$$\rho_t + (\rho v)_x = 0, \tag{3}$$

$$(v + p(\rho))_t + v(v + p(\rho))_x = \frac{V(\rho) - v}{\tau}, \tag{4}$$

where τ is the relaxation time. Without the relaxation term cars never reach the maximum allowable speed [9]. Note that at the equilibrium velocity this term is zero.

In vector form the ARZ model is

$$\begin{pmatrix} \rho \\ v \end{pmatrix}_t + \begin{pmatrix} v & \rho \\ 0 & v + \rho V'(\rho) \end{pmatrix} \begin{pmatrix} \rho \\ v \end{pmatrix}_x = \begin{pmatrix} 0 \\ \dfrac{V(\rho) - v}{\tau} \end{pmatrix}. \tag{5}$$

With the appropriate variable change, we can rewrite the model in the denisty-flow and velocity-flow forms, the latter of which is most useful to us for practical control purposes. Using the flow relation $q = \rho v$ and (5), the density-flow form is

$$\begin{pmatrix} \rho \\ q \end{pmatrix}_t + \begin{pmatrix} 0 & 1 \\ -\frac{q}{\rho}\left(\frac{q}{\rho} + \rho V'(\rho)\right) & 2\frac{q}{\rho} + \rho V'(\rho) \end{pmatrix} \begin{pmatrix} \rho \\ q \end{pmatrix}_x = \begin{pmatrix} 0 & 0 \\ \frac{V(\rho)}{\tau} & -\frac{1}{\tau} \end{pmatrix} \begin{pmatrix} \rho \\ q \end{pmatrix}. \tag{6}$$

In the same manner we arrive at the velocity-flow form,

$$\begin{pmatrix} v \\ q \end{pmatrix}_t + \begin{pmatrix} v + \frac{q}{v} V'\left(\frac{q}{v}\right) & 0 \\ \frac{q}{v}\left(v + \frac{q}{v} V'\left(\frac{q}{v}\right)\right) & v \end{pmatrix} \begin{pmatrix} v \\ q \end{pmatrix}_x = \frac{1}{\tau} \begin{pmatrix} V\left(\frac{q}{v}\right) - v \\ \frac{q}{v} V\left(\frac{q}{v}\right) - q \end{pmatrix}. \tag{7}$$

2.1. Linearization

We are interested only in small deviations, $(\tilde{\rho}(x,t), \tilde{v}(x,t))$, from the equilibrium. Consider the steady flow solution $(\rho^*(x), v^*(x))(V(\rho^*) = v^*)$. Then (5) becomes

$$v^* \frac{d\rho^*}{dx} + \frac{dv^*}{dx} \rho^* = 0, \tag{8}$$

$$(v^* + \rho^* V'(\rho^*)) \frac{dv^*}{dx} = \frac{V(\rho^*) - v^*}{\tau} = 0. \tag{9}$$

We must have $\frac{dv^*}{dx} = 0$ else $v^* + \rho^* V'(\rho^*) = 0$. Then we have also $\frac{d\rho^*}{dx} = 0$. Hence the steady-state solution is uniform along the road.

We linearize the ARZ model (5) about the steady-state described above. We obtain the linearized system

$$\begin{pmatrix} \tilde{\rho} \\ \tilde{v} \end{pmatrix}_t + \begin{pmatrix} v^* & \rho^* \\ 0 & v^* + \rho^* V'(\rho^*) \end{pmatrix} \begin{pmatrix} \tilde{\rho} \\ \tilde{v} \end{pmatrix}_x = \begin{pmatrix} 0 & 0 \\ \dfrac{V'(\rho^*)}{\tau} & -\frac{1}{\tau} \end{pmatrix} \begin{pmatrix} \tilde{\rho} \\ \tilde{v} \end{pmatrix} \tag{10}$$

Similarly for the density-flow system (6), we linearize about the equilibrium $(\rho^*, q^*)(\rho^* V(\rho^*) = q^*)$ with deviations $(\tilde{\rho}(x,t), \tilde{q}(x,t))$. The linearized system is as follows

$$\begin{pmatrix} \tilde{\rho} \\ \tilde{q} \end{pmatrix}_t + \begin{pmatrix} 0 & 1 \\ \alpha^*\beta^* & \alpha^* - \beta^* \end{pmatrix} \begin{pmatrix} \tilde{\rho} \\ \tilde{q} \end{pmatrix}_x = \begin{pmatrix} 0 & 0 \\ \delta & \sigma \end{pmatrix} \begin{pmatrix} \tilde{\rho} \\ \tilde{q} \end{pmatrix}, \tag{11}$$

where $\alpha^* = \frac{q^*}{\rho^*}$, $\beta^* = -\frac{q^*}{\rho^*} - \rho^* V'(\rho^*)$, $\delta = \dfrac{V(\rho^*) + \rho^* V'(\rho^*)}{\tau}$, and $\sigma = -\dfrac{1}{\tau}$.

Finally, for the velocity-flow system,

$$\begin{pmatrix} \tilde{v} \\ \tilde{q} \end{pmatrix}_t + \begin{pmatrix} v^* + \frac{q^*}{v^*} V'\left(\frac{q^*}{v^*}\right) & 0 \\ \frac{q^*}{v^*}\left(v^* + \frac{q^*}{v^*} V'\left(\frac{q^*}{v^*}\right)\right) & v^* \end{pmatrix} \begin{pmatrix} \tilde{v} \\ \tilde{q} \end{pmatrix}_x = \begin{pmatrix} -\dfrac{(v^*)^2 + q^* V'\left(\frac{q^*}{v^*}\right)}{(v^*)^2 \tau} & \dfrac{V'\left(\frac{q^*}{v^*}\right)}{v^* \tau} \\ -\dfrac{q^*\left((v^*)^2 + q^* V'\left(\frac{q^*}{v^*}\right)\right)}{(v^*)^3 \tau} & \dfrac{q^* V'\left(\frac{q^*}{v^*}\right)}{(v^*)^2 \tau} \end{pmatrix} \begin{pmatrix} \tilde{v} \\ \tilde{q} \end{pmatrix}. \tag{12}$$

2.2. Characteristic form

We rewrite the model in the characteristic form by diagonalizing the linearized equations. We begin with the density-flow system. Manipulating the equations in (10), we find

$$\begin{pmatrix}\zeta_1\\ \zeta_2\end{pmatrix}_t + \begin{pmatrix}\lambda_1 & 0\\ 0 & \lambda_2\end{pmatrix}\begin{pmatrix}\zeta_1\\ \zeta_2\end{pmatrix}_x = \begin{pmatrix}-\frac{1}{\tau} & 0\\ -\frac{1}{\tau} & 0\end{pmatrix}\begin{pmatrix}\zeta_1\\ \zeta_2\end{pmatrix}, \tag{13}$$

where $\zeta_1 = \tilde{v} - V'(\rho^*)\tilde{\rho}$ and $\zeta_2 = \tilde{v}$ are the characteristic variables of the (ρ, v) system, and $\lambda_1 = v^*$ and $\lambda_2 = v^* + \rho^* V'(\rho^*)$ are the eigenvalues. Note that $V'(\rho^*) < 0$ so $\lambda_2 \leq \lambda_1 = v^*$. Therefore this is consistent with the physical dynamics of the system as no waves travel faster than the equilibrium car speed.
We proceed in the same manner above to diagonalize the (ρ, q) system (11). The diagonal form is

$$\begin{pmatrix}\chi_1\\ \chi_2\end{pmatrix}_t + \begin{pmatrix}\lambda_1 & 0\\ 0 & \lambda_2\end{pmatrix}\begin{pmatrix}\chi_1\\ \chi_2\end{pmatrix}_x = \begin{pmatrix}-\frac{1}{\tau} & 0\\ -\frac{1}{\tau} & 0\end{pmatrix}\begin{pmatrix}\chi_1\\ \chi_2\end{pmatrix}, \tag{14}$$

where $\chi_1 = -\lambda_2\tilde{\rho} + \tilde{q}$ and $\chi_2 = -\lambda_1\tilde{\rho} + \tilde{q}$ are the characteristic variables in the (ρ, q) system and the eigenvalues λ_1 and λ_2 are the same as in the density-velocity system due to the relation $q^* = \rho^* v^*$.
Diagonalization of the velocity-flow system is more involved. Letting $\xi(x,t) = (\tilde{v}, \tilde{q})^T$, we can rewrite (12) as

$$\eta_t + A\eta_x = B\eta. \tag{15}$$

The eigenvalues of A are $\lambda_1 = v^*$ and $\lambda_2 = v^* + \frac{q^*}{v^*}V'\left(\frac{q^*}{v^*}\right)$, consistent with the previous systems. Then A can be diagonalized as follows

$$A = XDX^{-1}, \tag{16}$$

$$X = \begin{pmatrix}0 & \lambda_2 - \lambda_1\\ 1 & \rho^*\lambda_2\end{pmatrix}, \tag{17}$$

$$D = \begin{pmatrix}\lambda_1 & 0\\ 0 & \lambda_2\end{pmatrix}, \tag{18}$$

$$X^{-1} = \begin{pmatrix}\dfrac{\rho^*\lambda_2}{\lambda_1 - \lambda_2} & 1\\ -\dfrac{1}{\lambda_1 - \lambda_2} & 0\end{pmatrix}. \tag{19}$$

Define $\gamma(x,t) := X\eta(x,t)$. Hence (15) can be rewritten as

$$\gamma_t + \begin{pmatrix}\lambda_1 & 0\\ 0 & \lambda_2\end{pmatrix}\gamma_x = \begin{pmatrix}-\frac{1}{\tau} & 0\\ -\frac{1}{q^*\tau} & 0\end{pmatrix}\gamma \tag{20}$$

where

$$\gamma = \begin{pmatrix}\frac{\rho^*\lambda_2}{\lambda_1 - \lambda_2}\tilde{v} + \tilde{q}\\ -\frac{1}{\lambda_1 - \lambda_2}\tilde{v}\end{pmatrix}. \tag{21}$$

Let $\xi = (\chi_1, -q^*\chi_2)^T$. Then we have

$$\xi_t + \begin{pmatrix}\lambda_1 & 0\\ 0 & \lambda_2\end{pmatrix}\xi_x = \begin{pmatrix}-\frac{1}{\tau} & 0\\ -\frac{1}{\tau} & 0\end{pmatrix}\xi, \tag{22}$$

and

$$\xi = \begin{pmatrix}\dfrac{\rho^*\lambda_2}{\lambda_1 - \lambda_2}\tilde{v} + \tilde{q}\\ \dfrac{q^*}{\lambda_1 - \lambda_2}\tilde{v}\end{pmatrix} = \begin{pmatrix}\dfrac{\rho^*\lambda_2}{\lambda_1 - \lambda_2} & 1\\ \dfrac{\rho^*\lambda_1}{\lambda_1 - \lambda_2} & 0\end{pmatrix}\begin{pmatrix}\tilde{v}\\ \tilde{q}\end{pmatrix} \tag{23}$$

2.3. "Froude number"

In fluid mechanics the Froude number is a dimensionless number which delineates the boundary between flow regimes. Using the eigenvalues of the system in the characteristic form, we are able to define a useful analog to this number. Since $V(\rho)$ is nonincreasing function we have $V'(\rho^*) \leq 0$. Thus there are two flow regimes, where $\lambda_1\lambda_2 < 0$ and one characteristic curve travels downstream, and where $\lambda_1\lambda_2 > 0$ and both characteristic curves travel upstream.

Define $F := \dfrac{\rho^* V'(\rho^*)}{v^*}$. Then we have

$$\begin{cases} F > 1 & \Rightarrow |\rho^* V'(\rho^*)| > v^* \quad \Rightarrow \lambda_2 < 0 \\ F < 1 & \Rightarrow |\rho^* V'(\rho^*)| < v^* \quad \Rightarrow \lambda_2 > 0 \end{cases}.$$

Note also that $\lambda_2 = v^* + \rho^* V'(\rho^*) = \dfrac{Q(\rho^*)}{\rho^*} + \dfrac{\rho^* Q'(\rho^*) - Q(\rho^*)}{\rho^*} = Q'(\rho^*)$. Hence the system is in free flow when $F < 1$ and congestion when $F > 1$.

3. Frequency domain analysis

We consider only the (v, q) system for the frequency domain analysis for practical control purposes as described above.

3.1. State-transition matrix

In this section we analyze the linearized ARZ model in the frequency domain. For control purposes we are most interested in the (v, q) system.
Working with the (22) we obtain the following ODE

$$\frac{\partial \hat{\zeta}(x,s)}{\partial x} = \mathscr{A}(s)\hat{\zeta}(x,s) + \mathscr{B}\zeta(x, t = 0^-), \tag{24}$$

where $\mathscr{A}(s) = A^{-1}(B - sI)$ and $\mathscr{B} = -A^{-1}$. The general solution is

$$\hat{\zeta}(x,s) = \Phi(x,s)\hat{\zeta}(0,s) + \Phi(x,s)\int_0^x \Phi(v,s)^{-1}\mathscr{B}\zeta(v,0^-)dv, \tag{25}$$

where $\Phi(x,s) = e^{\mathscr{A}(s)x}$ is the state-transition matrix. Assuming zero initial conditions we have

$$\hat{\zeta}(x,s) = \Phi(x,s)\hat{\zeta}(0,s). \tag{26}$$

To compute the exponential we diagonalize the matrix as

$$\mathscr{A}(s) = \mathscr{X}(s)\mathscr{D}(s)\mathscr{X}^{-1}(s) \tag{27}$$

where

$$\mathscr{X}(s) = \begin{pmatrix} 0 & \dfrac{\lambda_2 - (\lambda_1 - \lambda_2)\tau s}{\lambda_1} \\ 1 & 1 \end{pmatrix}, \tag{28}$$

$$\mathscr{D}(s) = \begin{pmatrix} -\frac{s}{\lambda_2} & 0 \\ 0 & -\frac{1+\tau s}{\tau\lambda_1} \end{pmatrix}. \tag{29}$$

Hence

$$\Phi(x,s) = \mathscr{X}^{-1}(s)e^{\mathscr{D}(s)x}\mathscr{X}(s) = \begin{pmatrix} \phi_{11}(x,s) & \phi_{12}(x,s) \\ \phi_{21}(x,s) & \phi_{22}(x,s) \end{pmatrix}, \tag{30}$$

with

$$\phi_{11} = e^{-\frac{x}{\tau\lambda_1}} e^{-\frac{x}{\lambda_1}s}, \tag{31a}$$

$$\phi_{12} = 0, \tag{31b}$$

$$\phi_{21} = \frac{\lambda_1 \left(e^{-\frac{x}{\tau\lambda_1}} e^{-\frac{x}{\lambda_1}s} - e^{-\frac{x}{\lambda_2}s} \right)}{\lambda_2 - \tau(\lambda_1 - \lambda_2)s}, \tag{31c}$$

$$\phi_{22} = e^{-\frac{x}{\lambda_2}s}. \tag{31d}$$

3.2. Free flow case

Consider the system in the free flow regime. From (22) we see that ζ_1 travels with characteristic speed λ_1 and ζ_2 with characteristic speed λ_2. In the free flow regime we have $\lambda_1 \geq \lambda_2 > 0$, hence two boundary conditions are needed, both at the upstream boundary. A plot of the characteristics is shown in Figure 1.

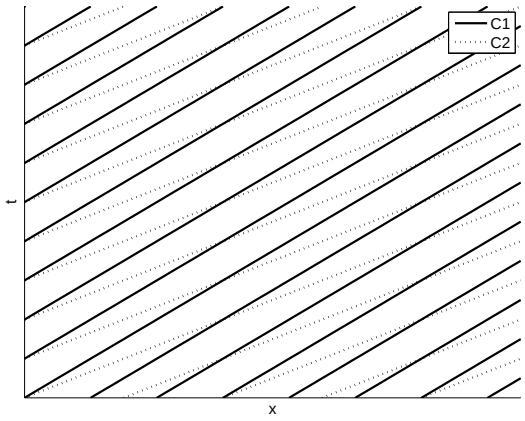

Figure 1: Illustration of the characteristics for supercritical flow, $\lambda_1 \geq \lambda_2 > 0$.

With $\zeta_1(0,t)$ and $\zeta_2(0,t)$ as the inputs and $\zeta_1(L,t)$ and $\zeta_2(L,t)$ as the outputs, the distributed transfer matrix is exactly the state-transition matrix $\Phi(x,s)$.

Using (23), we can write

$$\begin{pmatrix} \widetilde{v}(x,s) \\ \widetilde{q}(x,s) \end{pmatrix} = \underbrace{\begin{pmatrix} \frac{\rho^*\lambda_2}{\lambda_1-\lambda_2} & 1 \\ \frac{\rho^*\lambda_1}{\lambda_1-\lambda_2} & 0 \end{pmatrix}^{-1} \Phi(x,s) \begin{pmatrix} \frac{\rho^*\lambda_2}{\lambda_1-\lambda_2} & 1 \\ \frac{\rho^*\lambda_1}{\lambda_1-\lambda_2} & 0 \end{pmatrix}}_{\Psi(x,\,s)} \begin{pmatrix} \widetilde{v}(0,s) \\ \widetilde{q}(0,s) \end{pmatrix} \tag{32}$$

with

$$\psi_{11}(x,s) = \left(e^{-\frac{x}{\lambda_1\tau}} e^{-\frac{x}{\lambda_1}s} - e^{-\frac{x}{\lambda_2}s} \right) \frac{\alpha}{s+\alpha} + e^{-\frac{x}{\lambda_2}s}, \tag{33a}$$

$$\psi_{12}(x,s) = -\frac{1}{\rho^*\tau} \left(e^{-\frac{x}{\lambda_1\tau}} e^{-\frac{x}{\lambda_1}s} - e^{-\frac{x}{\lambda_2}s} \right) \frac{1}{s+\alpha}, \tag{33b}$$

$$\psi_{21}(x,s) = -\rho^*\tau \left(e^{-\frac{x}{\lambda_1\tau}} e^{-\frac{x}{\lambda_1}s} - e^{-\frac{x}{\lambda_2}s} \right) \frac{\alpha s}{s+\alpha}, \tag{33c}$$

$$\psi_{22}(x,s) = -\left(e^{-\frac{x}{\lambda_1\tau}} e^{-\frac{x}{\lambda_1}s} - e^{-\frac{x}{\lambda_2}s} \right) \frac{\alpha}{s+\alpha} + e^{-\frac{x}{\lambda_1\tau}} e^{-\frac{x}{\lambda_1}s}. \tag{33d}$$

where $\alpha = -\dfrac{\lambda_2}{\tau(\lambda_1 - \lambda_2)}$.

3.2.1. Bode plots

We generate Bode plots using the following parameters taken from [10]: $q_{max} = 1300$ veh/h, $\rho_{max} = 0.1$ veh/m, and $L = 100$ m: The Greenshields Hamiltonian, $Q(\rho) = 4\frac{q_{max}}{\rho_{max}^2}\rho(\rho_{max} - \rho)$, is used to approximate the fundamental diagram. For inhomogenous second-order models, the relaxation time, τ, falls in the range of about 14-60 seconds [11]. A relaxation time of $\tau = 15$ s is used for the following simulations. We simulate for $\rho^* = 0.01$.

For the physical variables:

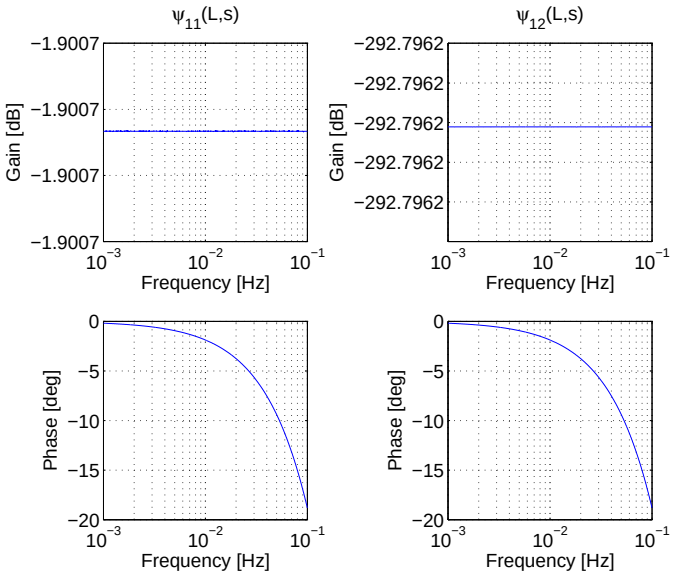

Figure 2: Bode magnitude and phase plots for $\psi_{11}(L, s)$ and $\psi_{12}(L, s)$.

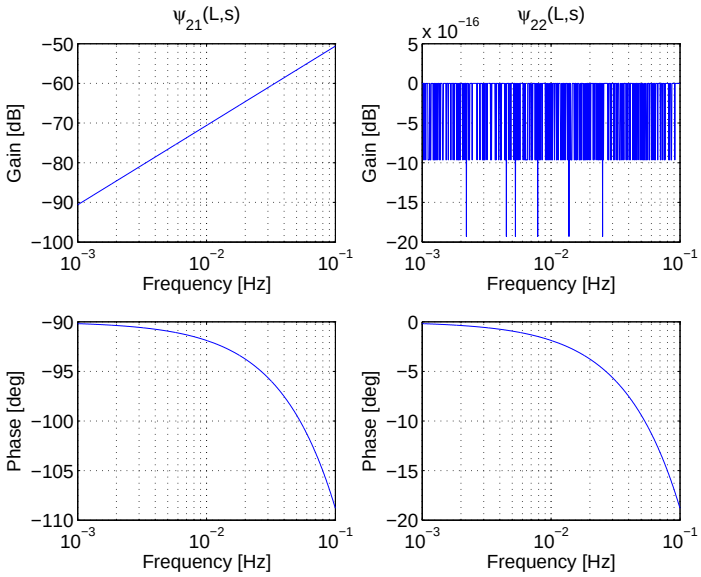

Figure 3: Bode magnitude and phase plots for $\psi_{21}(L, s)$ and $\psi_{22}(L, s)$.

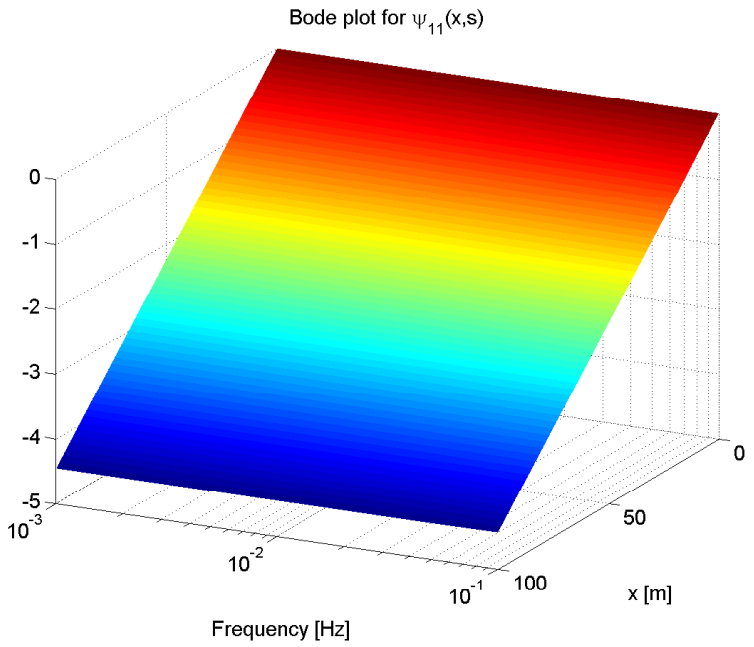

Figure 4: Spatial Bode magnitude plot for $\psi_{11}(x, s)$.

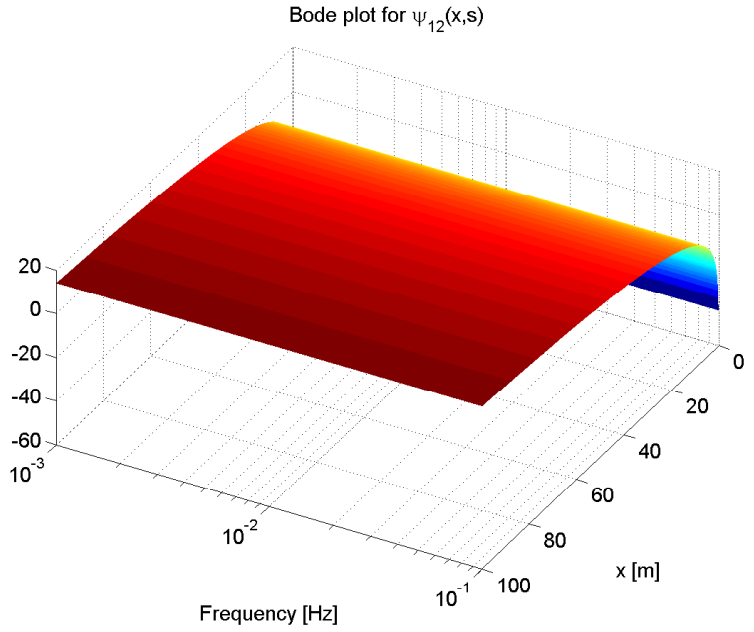

Figure 5: Spatial Bode magnitude plot for $\psi_{12}(x, s)$.

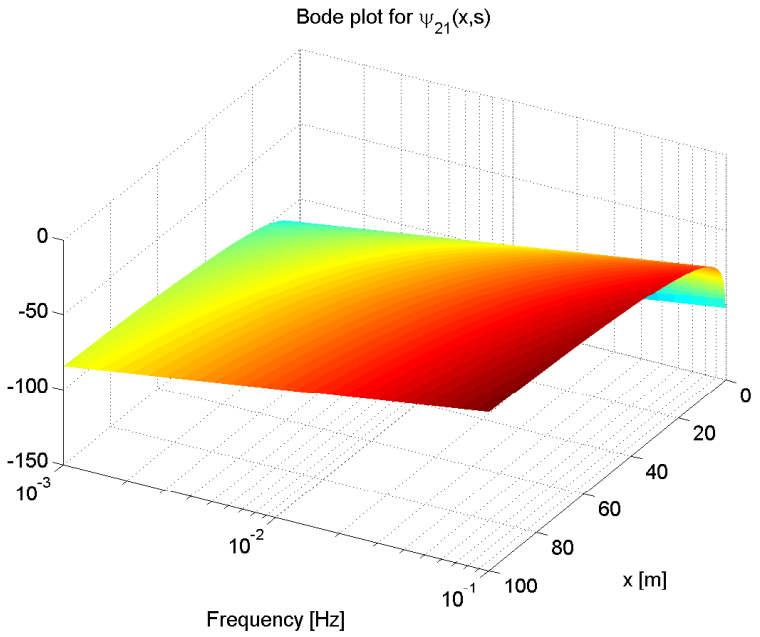

Figure 6: Spatial Bode magnitude plot for $\psi_{21}(x, s)$.

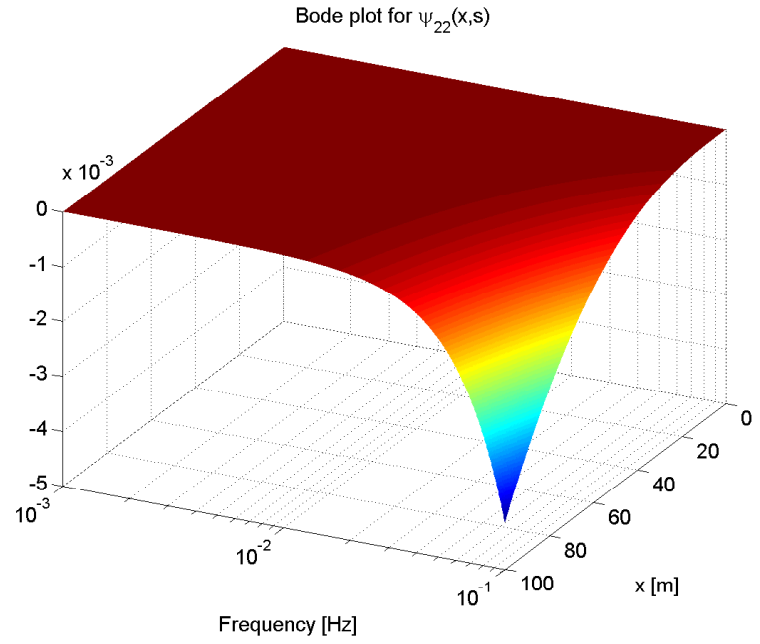

Figure 7: Spatial Bode magnitude plot for $\psi_{22}(x, s)$.

For the Riemann invariants:

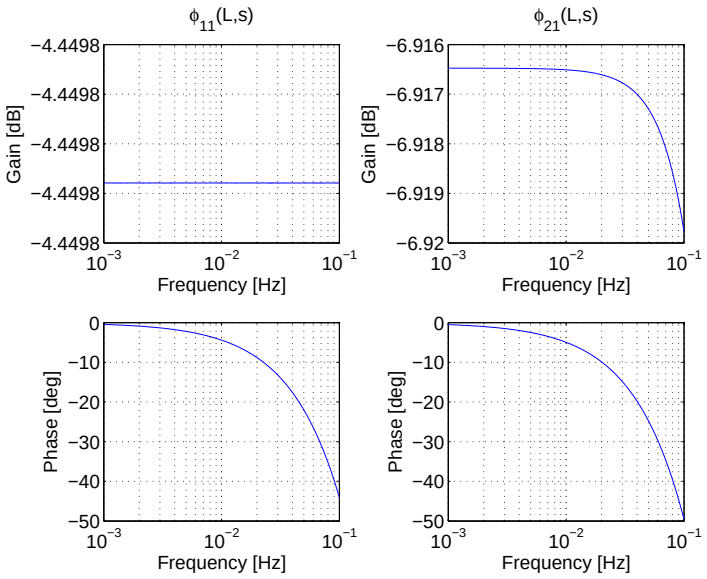

Figure 8: Bode magnitude and phase plots for $\phi_{11}(L, s)$ and $\phi_{21}(L, s)$.

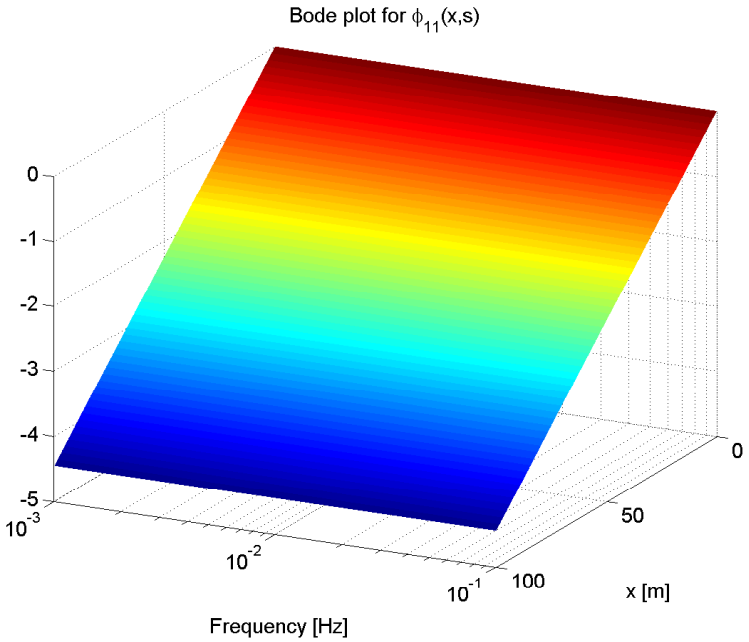

Figure 9: Spatial Bode magnitude plot for $\phi_{11}(x, s)$.

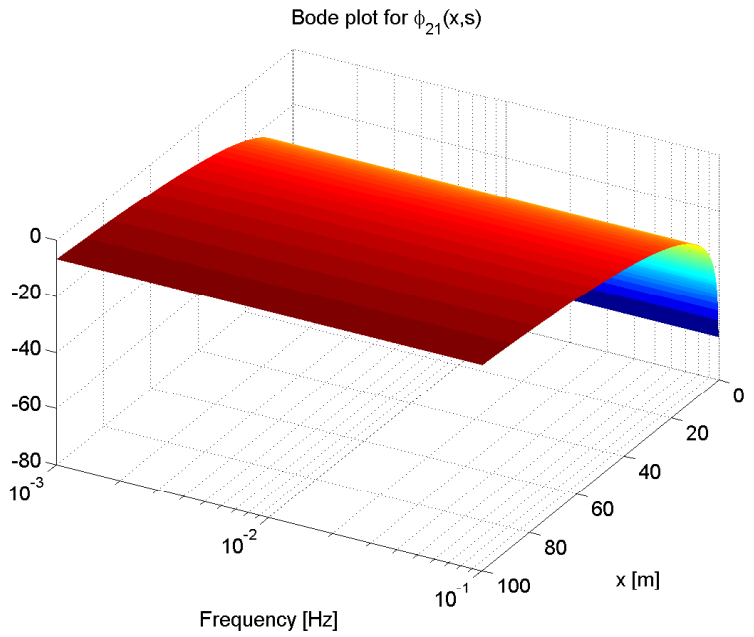

Figure 10: Spatial Bode magnitude plot for $\phi_{21}(x, s)$.

3.2.2. Step responses

We analyze the behavior of the system given step inputs $v(0,t) = v_{step}H(t)$ and $q(0,t) = q_{step}H(t)$, where $H(\cdot)$ is the Heaviside function. The step responses are

$$\begin{aligned} v(x,t) = v_{step} &\left[e^{-\frac{x}{\lambda_1 \tau}}\left(1 - e^{-a\left(t-\frac{x}{\lambda_1}\right)}\right) H\left(t - \frac{x}{\lambda_1}\right) + e^{-a\left(t-\frac{x}{\lambda_2}\right)} H\left(t - \frac{x}{\lambda_2}\right)\right] \\ &+ \frac{q_{step}}{\rho^* \tau}\left[-e^{-\frac{x}{\lambda_1 \tau}}\left(1 - e^{-a\left(t-\frac{x}{\lambda_1}\right)}\right) H\left(t - \frac{x}{\lambda_1}\right) + \left(1 - e^{-a\left(t-\frac{x}{\lambda_2}\right)}\right) H\left(t - \frac{x}{\lambda_2}\right)\right] \end{aligned} \tag{34}$$

$$\begin{aligned} q(x,t) = v_{step}\rho^* \tau a &\left[e^{-\frac{x}{\lambda_1 \tau}} e^{-a\left(t-\frac{x}{\lambda_1}\right)} H\left(t - \frac{x}{\lambda_1}\right) - e^{-a\left(t-\frac{x}{\lambda_2}\right)} H\left(t - \frac{x}{\lambda_2}\right)\right] \\ &+ q_{step}\left[e^{-\frac{x}{\lambda_1 \tau}} e^{-a\left(t-\frac{x}{\lambda_1}\right)} H\left(t - \frac{x}{\lambda_1}\right) + \left(1 - e^{-a\left(t-\frac{x}{\lambda_2}\right)}\right) H\left(t - \frac{x}{\lambda_2}\right)\right] \end{aligned} \tag{35}$$

3.3. Congested flow

Consider now the system in the congestion flow regime. Here we have $\lambda_1 > 0, \lambda_2 < 0$, hence two boundary conditions are needed, one at the upstream boundary and one at the downstream boundary. A plot of the characteristics is shown in Figure 11.

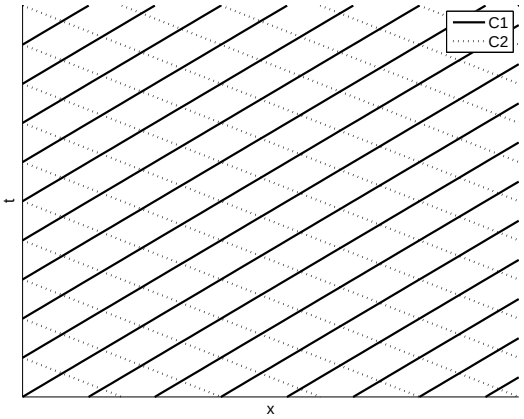

Figure 11: Illustration of the characteristics for supercritical flow, $\lambda_1 > 0, \lambda_2 < 0$.

Using (26) we can write

$$\begin{pmatrix} \hat{\xi_1}(x,s) \\ \hat{\xi_2}(x,s) \end{pmatrix} = \underbrace{\Phi(x,s) \begin{pmatrix} 1 & 0 \\ -\frac{\phi_{21}(L,s)}{\phi_{22}(L,s)} & \frac{1}{\phi_{22}} \end{pmatrix}}_{\Gamma(x,s)} \begin{pmatrix} \hat{\xi_1}(0,s) \\ \hat{\xi_2}(0,s) \end{pmatrix}. \tag{36}$$

with

$$\gamma_{11}(x,s) = e^{-\frac{x}{\lambda_1 \tau}} e^{-\frac{sx}{\lambda_1}}, \tag{37a}$$

$$\gamma_{12}(x,s) = 0, \tag{37b}$$

$$\gamma_{21}(x,s) = \alpha \frac{\lambda_1}{\lambda_2} \left(e^{-\frac{x}{\lambda_1 \tau}} e^{-\frac{sx}{\lambda_1}} - e^{-\frac{L}{\lambda_1 \tau}} e^{-\frac{s}{\lambda_2}\left(x - L\frac{\lambda_1 - \lambda_2}{\lambda_1}\right)} \right) \frac{1}{s+\alpha}, \tag{37c}$$

$$\gamma_{22}(x,s) = e^{-\frac{s(x-L)}{\lambda_2}}. \tag{37d}$$

4. Numerical validation

- Values for parameters (τ?)
- Convergence towards equilibrium of trajectories in (v, q) domain
- Spectral transform of data and response

5. Results/discussion

6. Conclusion

[further steps]

Acknowledgments

References

[1] D. Schrank, B. Eisele, , T. Lomax, Urban mobility report, Tech. rep., Texas A and M Transportation Institute (2012).

[2] M. J. Lighthill, J. B. Whitham, On kinematic waves. II: A theory of traffic flow on long crowded roads., Proc. Royal. Soc. (1955) 317–345.

[3] P. I. Richards, Shock waves on the highway, Operations Research 4 (1) (1956) pp. 42–51.

[4] H. J. Payne, Models of Freeway Traffic and Control, Simulation Councils, Incorporated, 1971.

[5] G. B. Whitham, Linear and Nonlinear Waves, A Wiley-Interscience publication, Wiley, 1974.

[6] C. Daganzo, Requiem for second-order fluid approximations of traffic flow, Transportation Res. Part B 29 (4) (1995) 277–286.

[7] A. Aw, M. Rascle, Resurrection of second order models of traffic flow, SIAM Journal of Applied Mathematics 60 (3) (2000) 916–938.

[8] H. M. Zhang, A non-equilibrium traffic model devoid of gas-like behavior, Transportation Res. Part B 36 (2002) 275–290.

[9] M. Rascle, An improved macroscopic model of traffic flow: derivation and links with the lighthill-whitham model, Mathematical and computer modelling 35 (2002) 581–590.

[10] A. Hofleitner, C. Claudel, A. Bayen, Reconstruction of boundary conditions from internal conditions using viability theory, in: American Control Conference, IEEE, 2012, pp. 640–645.

[11] S. Fan, M. Herty, B. Seibold, Comparative model accuracy of a data-fitted generalized aw-rascle-zhang model, Networks and Heterogeneous Media 9 (2) (2014) 239–268.